Supplementary Information (SI) for Physical Chemistry Chemical Physics.

Supporting Information: Free Energy Landscapes of Host-Guest Binding from Adaptive Bias Enhanced Sampling

Revanth Elangovan[†] and Dhiman Ray[*,†,‡]

†*Department of Chemistry and Biochemistry, University of Oregon, Eugene, Oregon 97403, USA*

‡*Material Science Institute, University of Oregon, Eugene, Oregon 97403, USA*

E-mail: dray@uoregon.edu

1 Supplementary Methods

1.1 Simulation parameters of Well-Tempered Metadynamics (WT-MetaD) simulations for barrier height estimation

To estimate the energy barrier for host–guest systems, we performed 10 independent Well-Tempered Metadynamics simulations and sampled the guest's unbinding from the host. The parameters used for the WT-MetaD calculations were: bias factor $\gamma = 10$, Gaussian width $\sigma = 0.05$, initial Gaussian height $W_0 = 1.2$ kJ mol^{-1}, and deposition stride PACE = 1 ps.

1.2 Simulation Parameters for OPES$_{\mathrm{COM}}$

The `BARRIER` parameter ΔE for the OPES$_{\mathrm{COM}}$ simulations of the OAH host systems with all six guests and two different CV combinations is provided below. The ΔE parameters for the OPES$_{\mathrm{COM}}$ simulations of the OAMe host with the 2D CV space are identical to the parameters for the 1D CV space provided in Table 1 of the main text. All simulations used a bias deposition interval of 1 ps.

Table S1: Choice of the `BARRIER` (ΔE) parameters for the OPES$_{\mathrm{COM}}$ from the maximum bias deposited in one-way WT-MetaD simulations sampling unbinding transitions. The maximum bias and its uncertainty have been computed from 10 independent WT-MetaD runs. This table shows the data for the six guests and the OAH host with z CV.

System	Estimated barrier height from WT-MetaD (kJ/mol)	ΔE (OPES) (kJ/mol)	ΔE (OPES$_e$) (kJ/mol)
OAH-G1	51 ± 8	50	28
OAH-G2	41 ± 7	40	25
OAH-G3	50 ± 13	50	28
OAH-G4	80 ± 7	80	45
OAH-G5	45 ± 9	45	25
OAH-G6	52 ± 10	50	28

Table S2: Choice of the `BARRIER` (ΔE) parameters for the OPES_{COM} from the maximum bias deposited in one-way WT-MetaD simulations sampling unbinding transitions. The maximum bias and its uncertainty have been computed from 10 independent WT-MetaD runs. This table shows the data for the six guests and the OAH host with z and $V2$ as CVs.

System	Estimated barrier height from WT-MetaD (kJ/mol)	ΔE (OPES) (kJ/mol)	ΔE (OPES_e) (kJ/mol)
OAH-G1	49 ± 6	50	28
OAH-G2	39 ± 6	40	25
OAH-G3	41 ± 6	40	25
OAH-G4	69 ± 10	70	38
OAH-G5	41 ± 11	40	25
OAH-G6	47 ± 4	50	28

1.3 Neural Network Training Parameters

The Deep-TDA CVs for reference simulations for all the host–guest systems were trained using the same neural network architecture with a 12-8-8-1 topology. In all cases, the 12 water coordination numbers were employed as input descriptors after normalization. The target distribution was defined with centers at -5 (bound state) and 5 (unbound state), and a Gaussian width (σ) of 0.2 for each state.

2 Supplementary Results

2.1 Convergence - OPES Simulations

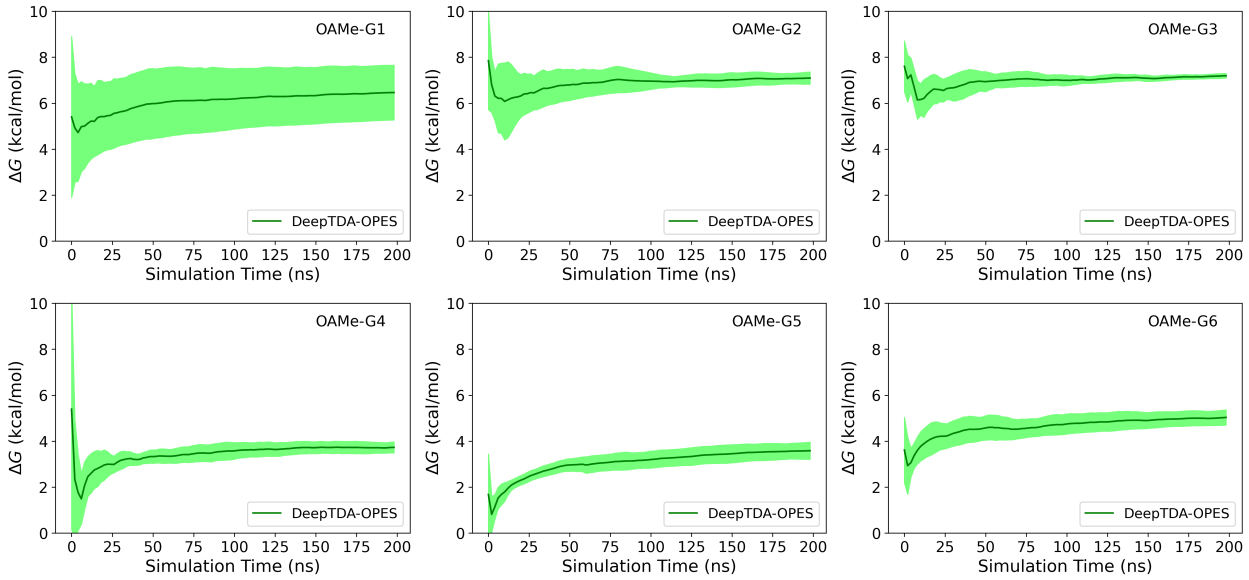

Figure S1: Convergence of the reference binding free energy values computed from OPES simulations using z and Deep-TDA CVs. The green-shaded region depicts a 95% confidence interval based on four independent runs of all six guest molecules with the OAMe host.

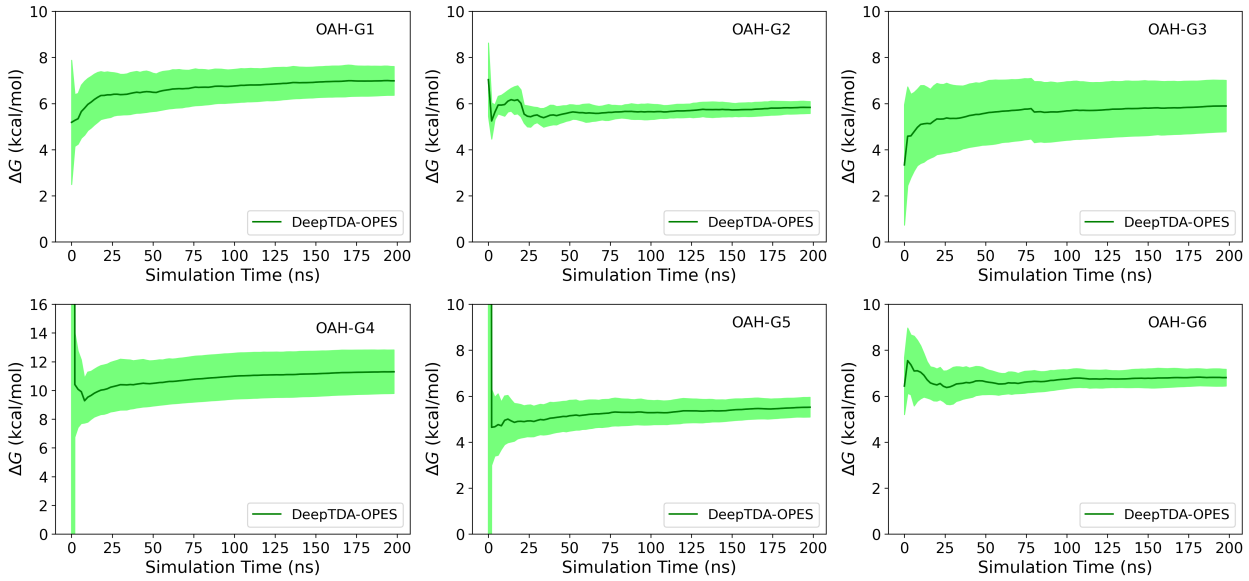

Figure S2: Same as Fig. S1 except for the OAH host.

2.2 A note on performing OPES$_{\mathrm{COM}}$ simulation in a 2D CV space.

When both CVs (z and $V2$) were biased for OPES and the OPES$_e$ component in the OPES$_{\mathrm{COM}}$ simulations, the OPES$_e$ bias increased sharply at the beginning of the simulation before becoming comparable to the OPES bias (Fig. S3). This artifact led to difficulties in converging the free energy values. Ideally, for a successful OPES$_{\mathrm{COM}}$ simulation, the bias deposited from the OPES and the OPES$_e$ component needs to be similar or comparable. We therefore biased only the z CV in the OPES$_e$ component of the OPES$_{\mathrm{COM}}$ simulations when using a 2D CV space, such as z and $V2$. This kept the OPES$_e$ bias stable without overshooting the OPES bias (Fig. S3, leading to improved sampling and well-converged free energy estimates. Therefore, for all systems in the OAMe and OAH sets, we biased only the z CV in the OPES$_e$ component of the OPES$_{\mathrm{COM}}$ simulations.

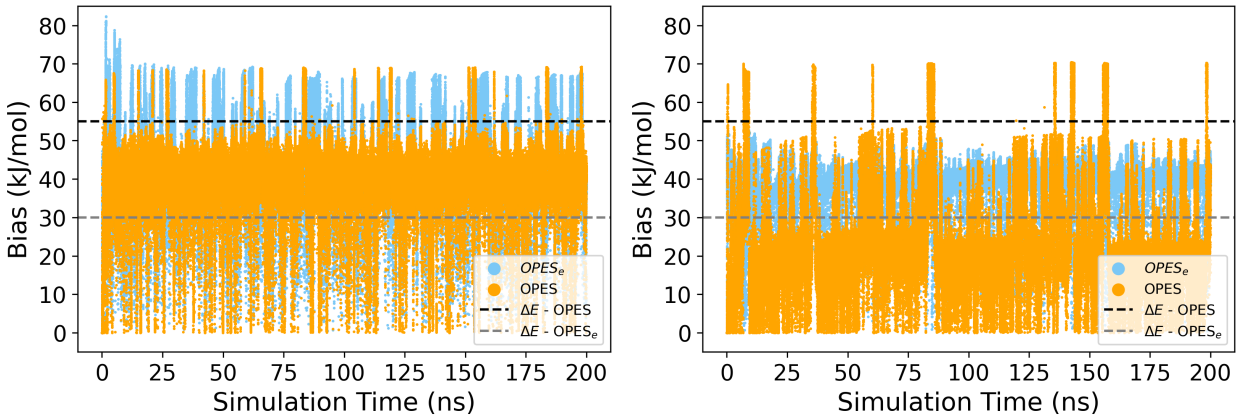

Figure S3: Bias deposition by the OPES and OPES$_e$ components of OPES$_{\mathrm{COM}}$ simulations for the OAMe-G2 system. Left panel: both CVs (z and V_2) are biased. Right panel: only the z CV is biased in the OPES$_e$ part of the OPES$_{\mathrm{COM}}$ simulations.

2.3 Results of OPES and OPES$_e$ simulations using only z CV for the OAMe-G2 complex

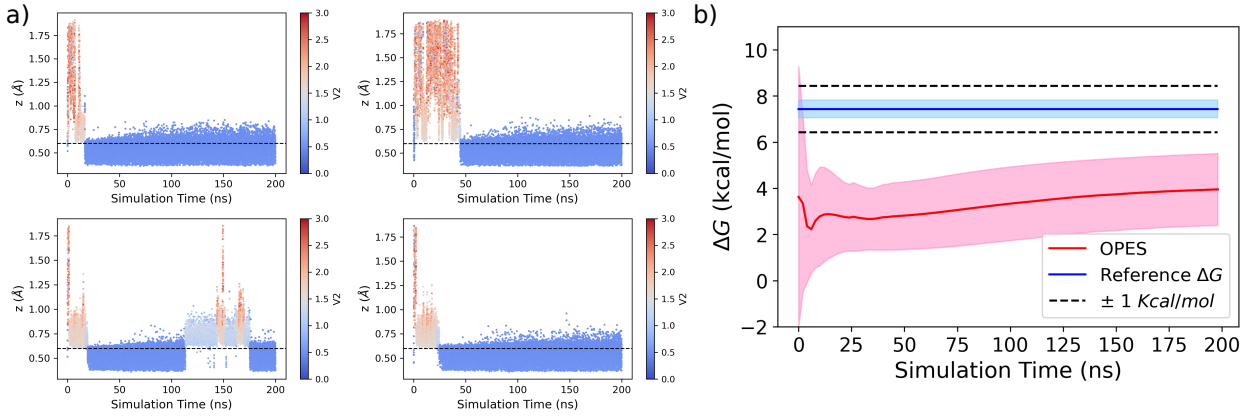

Figure S4: (a) Transitions sampled between the bound and unbound states across the four independent and (b) Convergence of the binding free energy estimates obtained from the OPES simulations for the OAMe-G2 system.

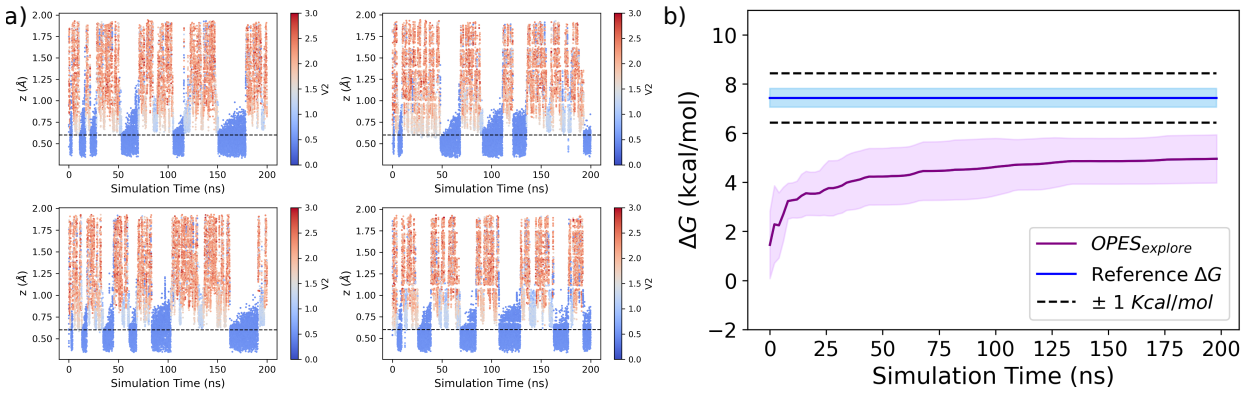

Figure S5: (a) Transitions sampled between the bound and unbound states across the four independent and (b) Convergence of the binding free energy estimates obtained from the OPES$_e$ simulations for the OAMe-G2 system.

2.4 OAMe-G1

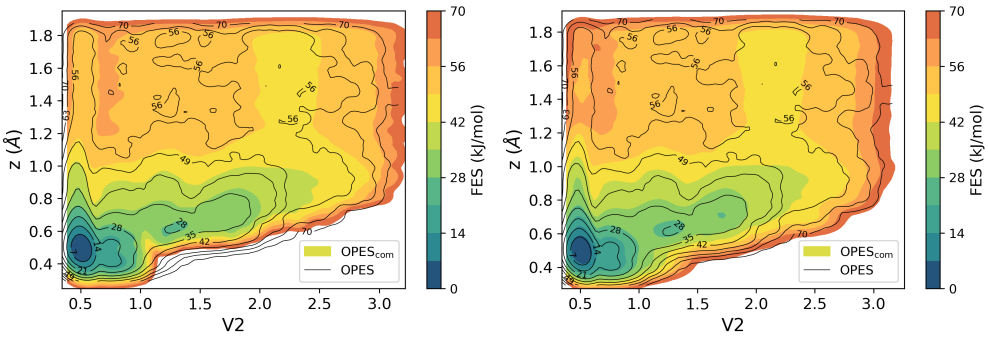

Figure S6: Results of the free energy landscape for the G1 guest binding to the OAMe host. The free energy surfaces (FES) projected along the 2D CV space consisting of the z distance and the $V2$ water coordination. Colored contours represent the FES obtained from OPES$_{\mathrm{COM}}$ simulations with bias deposition along (left pannel) only z and (right pannel) z and $V2$. The black contours represent the reference FES computed using OPES simulations using z and Deep-TDA CV.

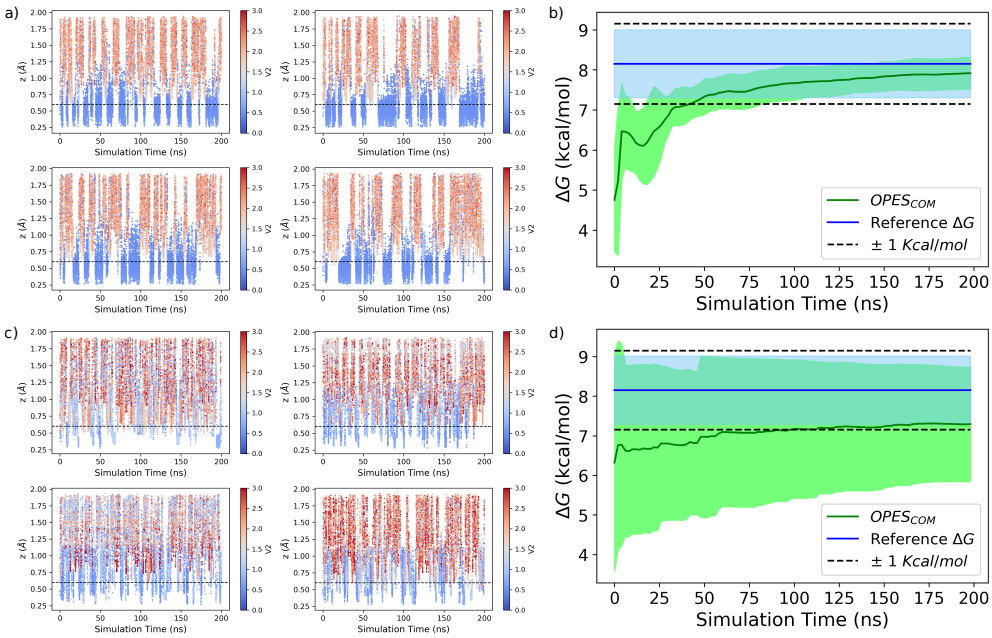

Figure S7: Back and forth transitions between the bound and the unbound states for the four independent OPES$_{\mathrm{COM}}$ simulations with bias deposition along (a) only z and (c) z and $V2$. The location of the bound state is shown in a black dashed line. Convergence of the binding free energies from OPES$_{\mathrm{COM}}$ simulations using (b) only z and (d) z and $V2$ CVs. The green-shaded region depicts a 95% confidence interval from four independent runs

2.5 OAMe-G2

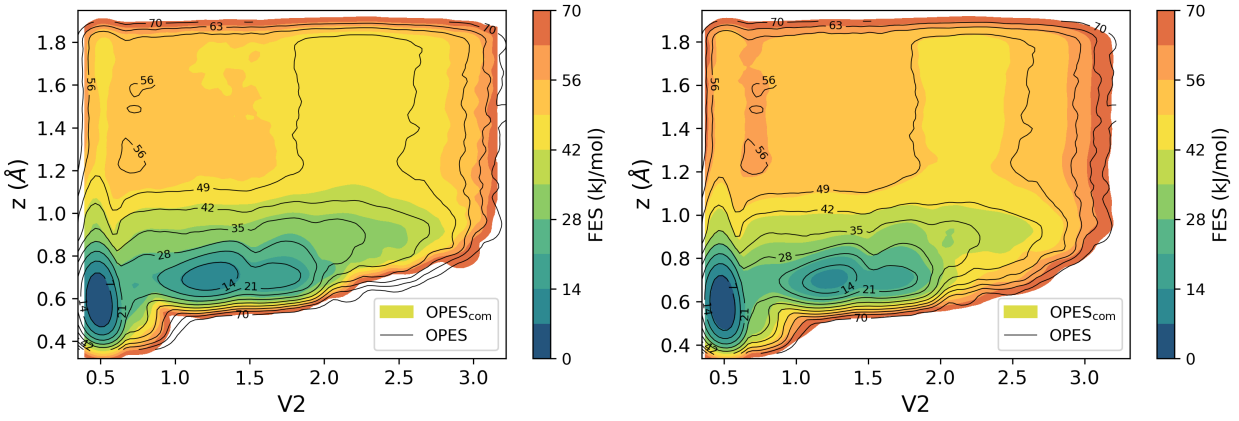

Figure S8: Results of the free energy landscape for the G2 guest binding to the OAMe host. The captions of the subfigures are identical to Fig. S6

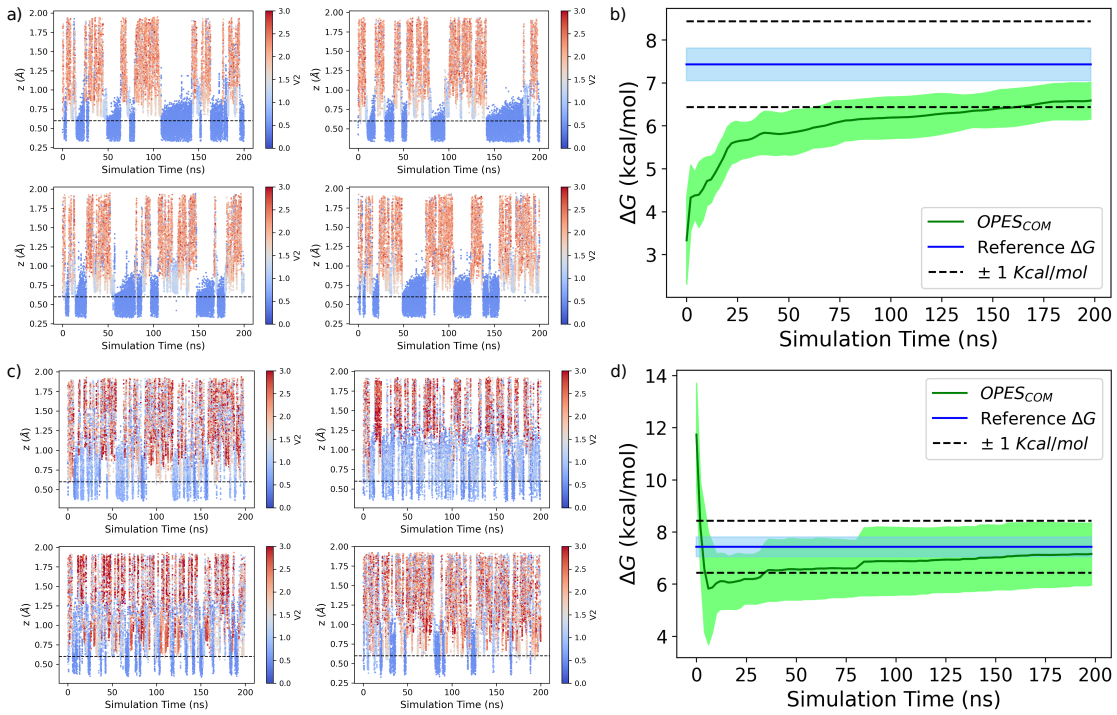

Figure S9: Back–and–forth transitions between the bound and unbound states for all the OPES$_{COM}$ simulations, along with the corresponding convergence profiles of the binding free energies. The subfigure captions are identical to Fig.S7

2.6 OAMe-G3

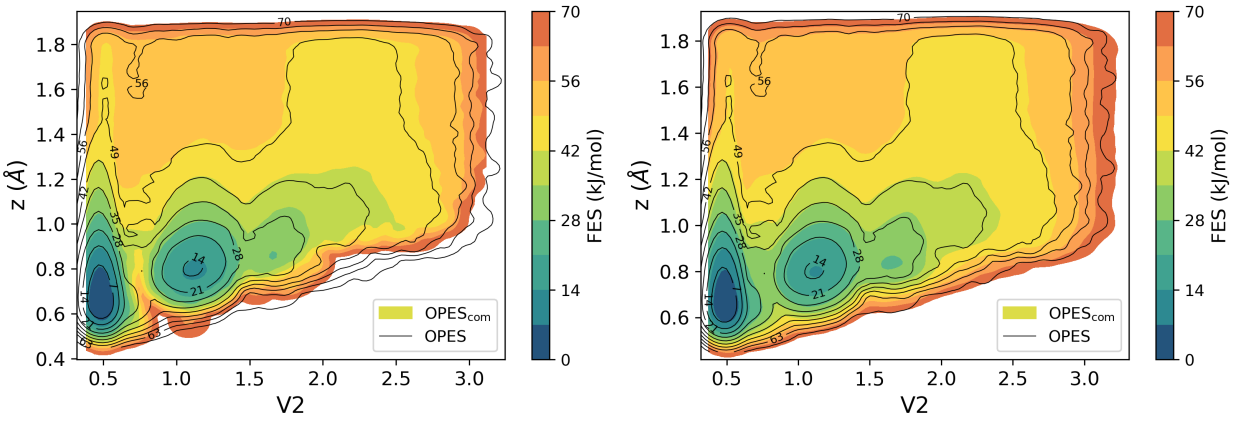

Figure S10: Results of the free energy landscape for the G3 guest binding to the OAMe host. The captions of the subfigures are identical to Fig. S6

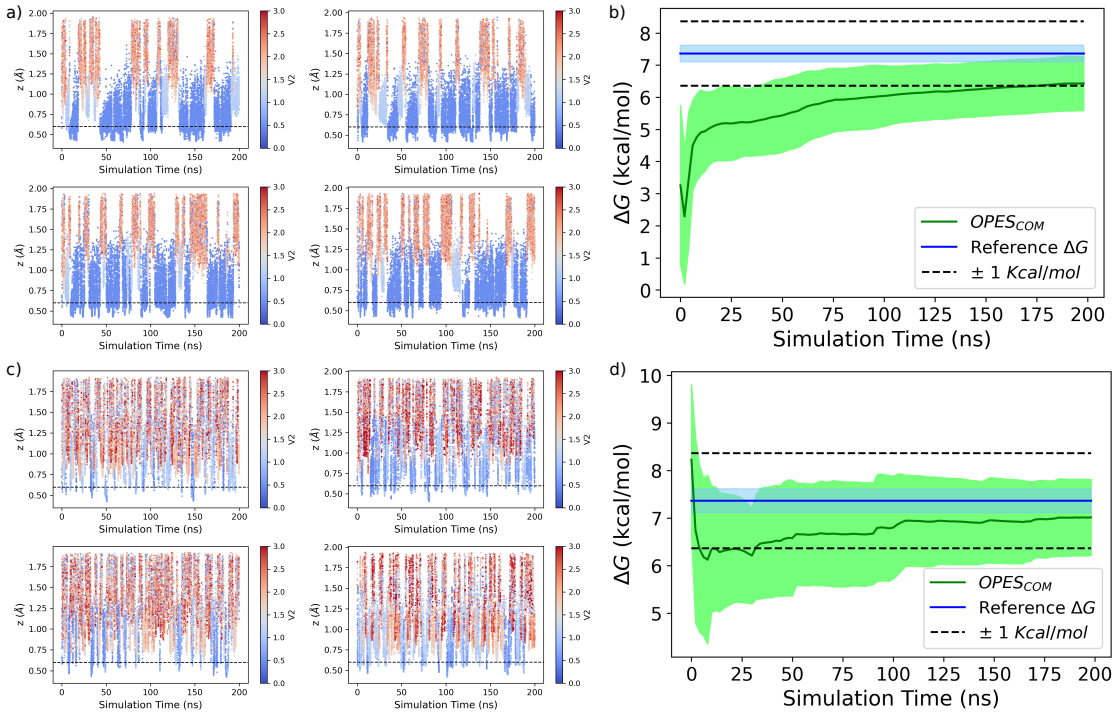

Figure S11: Back–and–forth transitions between the bound and unbound states for all the OPES$_{COM}$ simulations, along with the corresponding convergence profiles of the binding free energies. The subfigure captions are identical to Fig.S7

2.7 OAMe-G4

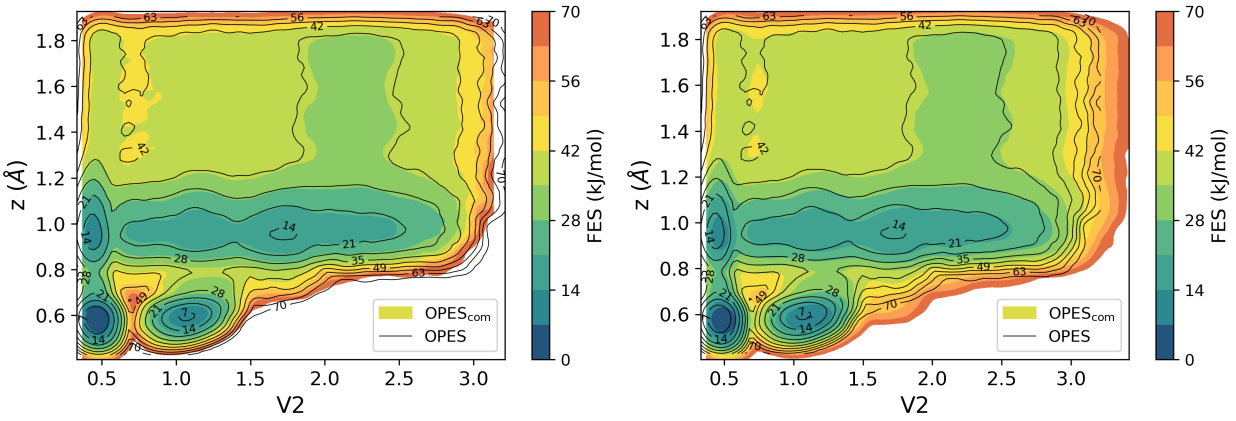

Figure S12: Results of the free energy landscape for the G4 guest binding to the OAMe host. The captions of the subfigures are identical to Fig. S6

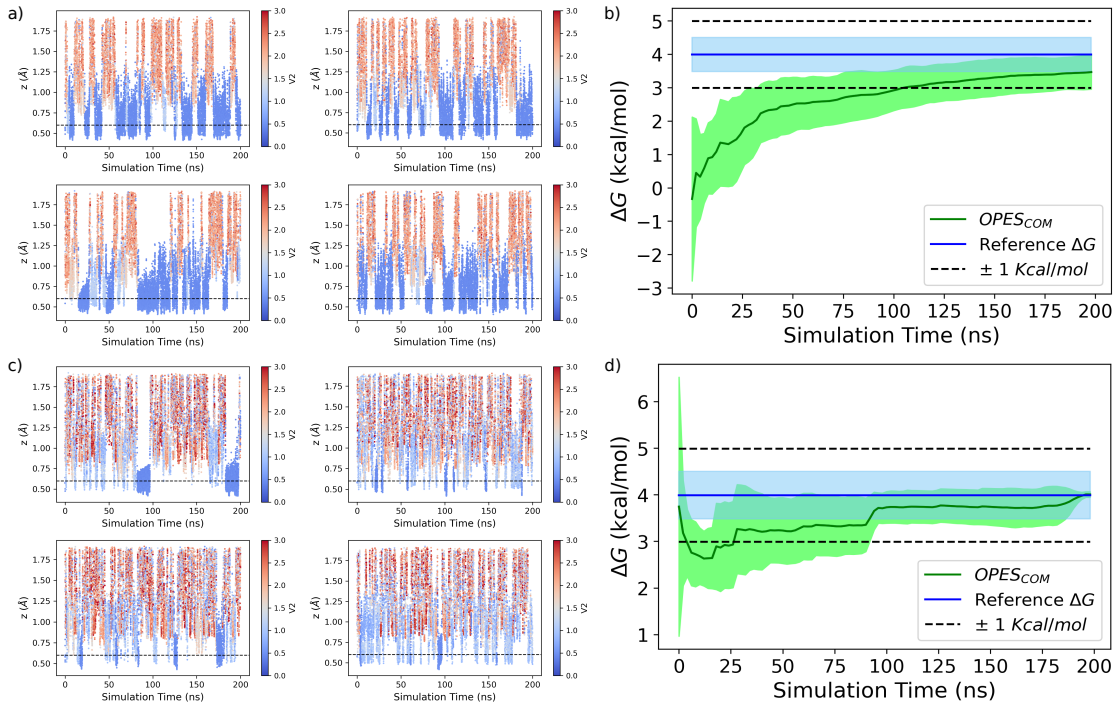

Figure S13: Back–and–forth transitions between the bound and unbound states for all the OPES_{COM} simulations, along with the corresponding convergence profiles of the binding free energies. The subfigure captions are identical to Fig.S7

2.8 OAMe-G5

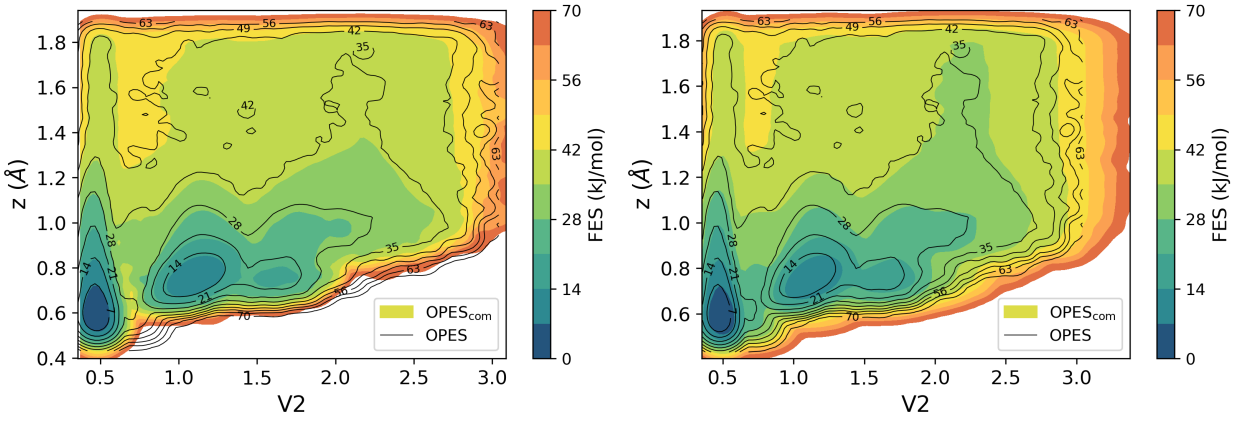

Figure S14: Results of the free energy landscape for the G5 guest binding to the OAMe host. The captions of the subfigures are identical to Fig. S6

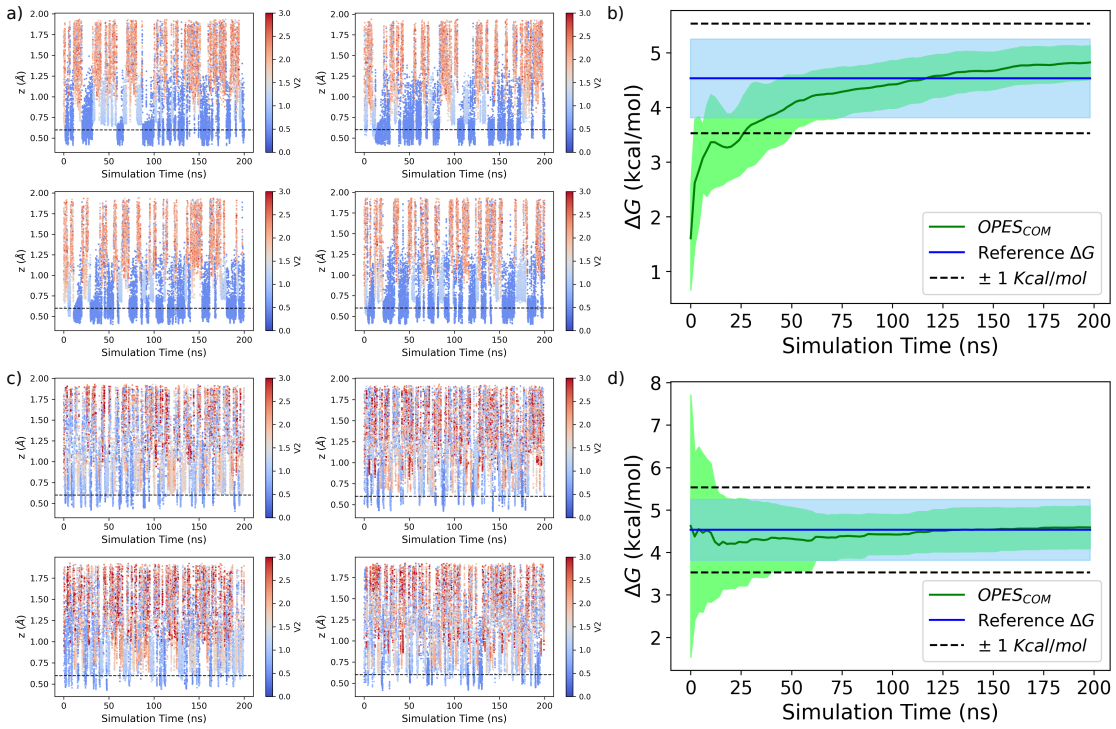

Figure S15: Back–and–forth transitions between the bound and unbound states for all the OPES_{COM} simulations, along with the corresponding convergence profiles of the binding free energies. The subfigure captions are identical to Fig.S7

2.9 OAMe-G6

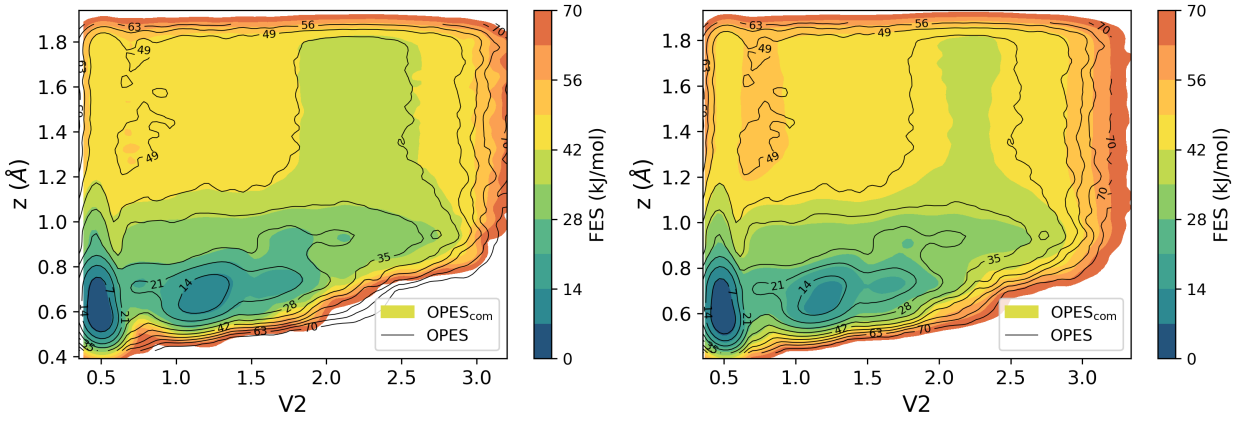

Figure S16: Results of the free energy landscape for the G6 guest binding to the OAMe host. The captions of the subfigures are identical to Fig. S6

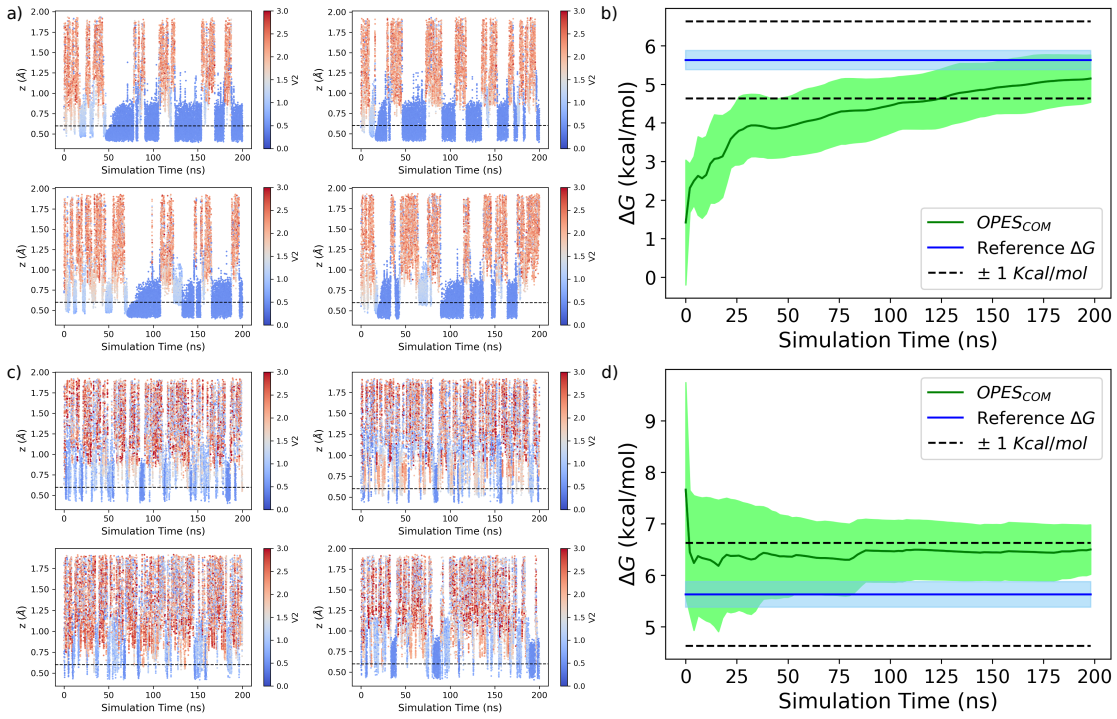

Figure S17: Back–and–forth transitions between the bound and unbound states for all the OPES$_{\text{COM}}$ simulations, along with the corresponding convergence profiles of the binding free energies. The subfigure captions are identical to Fig.S7

2.10 OAH-G1

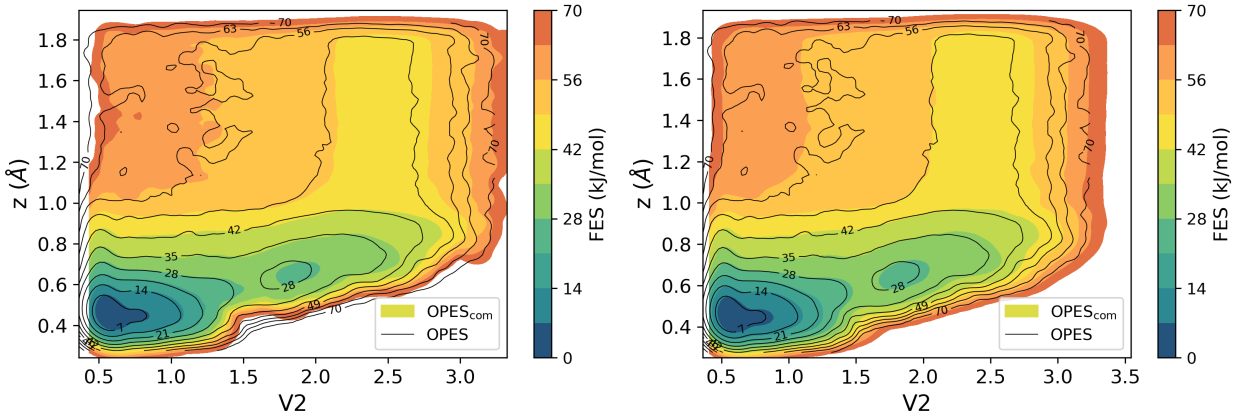

Figure S18: Results of the free energy landscape for the G1 guest binding to the OAH host. The captions of the subfigures are identical to Fig. S6

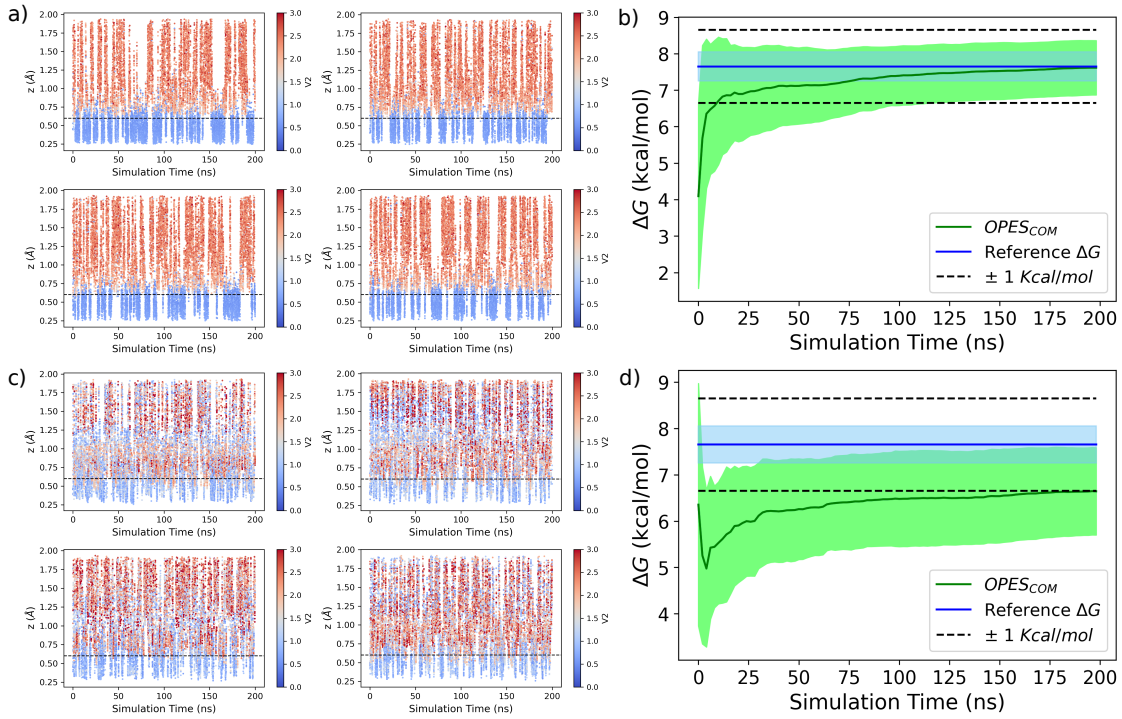

Figure S19: Back–and–forth transitions between the bound and unbound states for all the OPES$_{COM}$ simulations, along with the corresponding convergence profiles of the binding free energies. The subfigure captions are identical to Fig.S7

2.11 OAH-G2

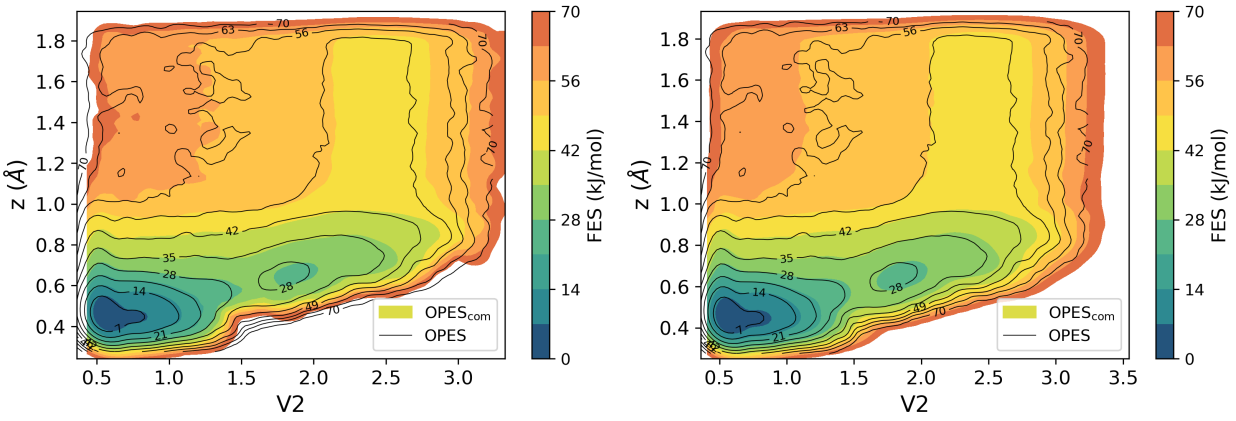

Figure S20: Results of the free energy landscape for the G2 guest binding to the OAH host. The captions of the subfigures are identical to Fig. S6

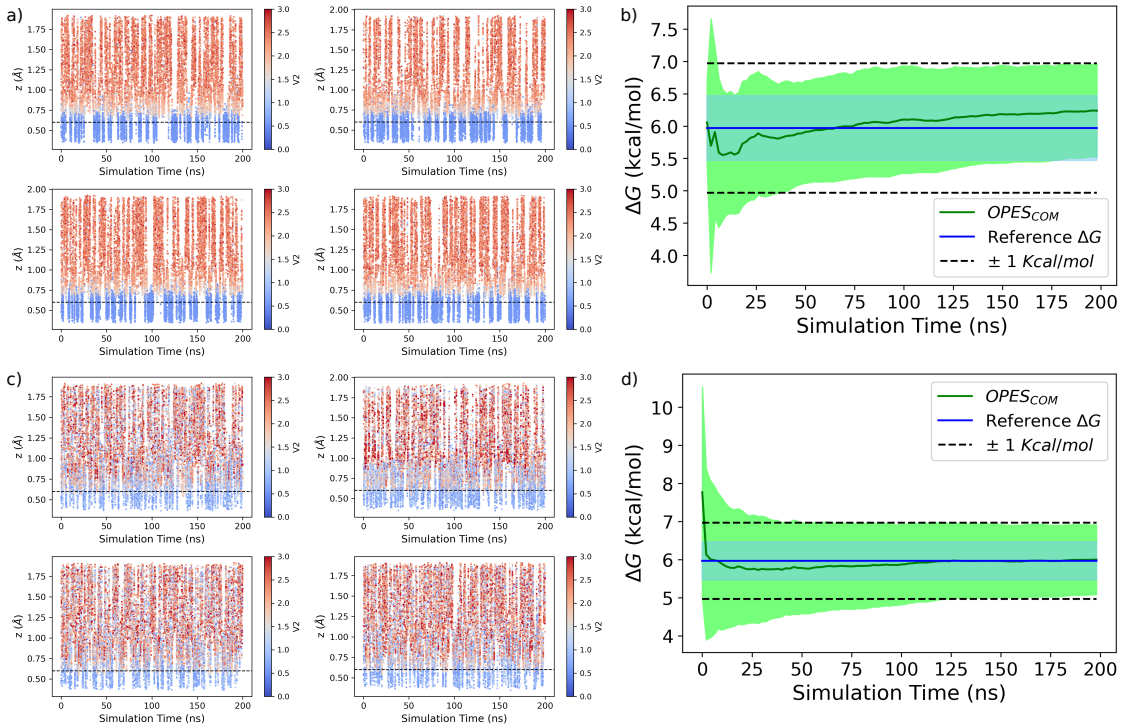

Figure S21: Back–and–forth transitions between the bound and unbound states for all the OPES_{COM} simulations, along with the corresponding convergence profiles of the binding free energies. The subfigure captions are identical to Fig.S7

2.12 OAH-G3

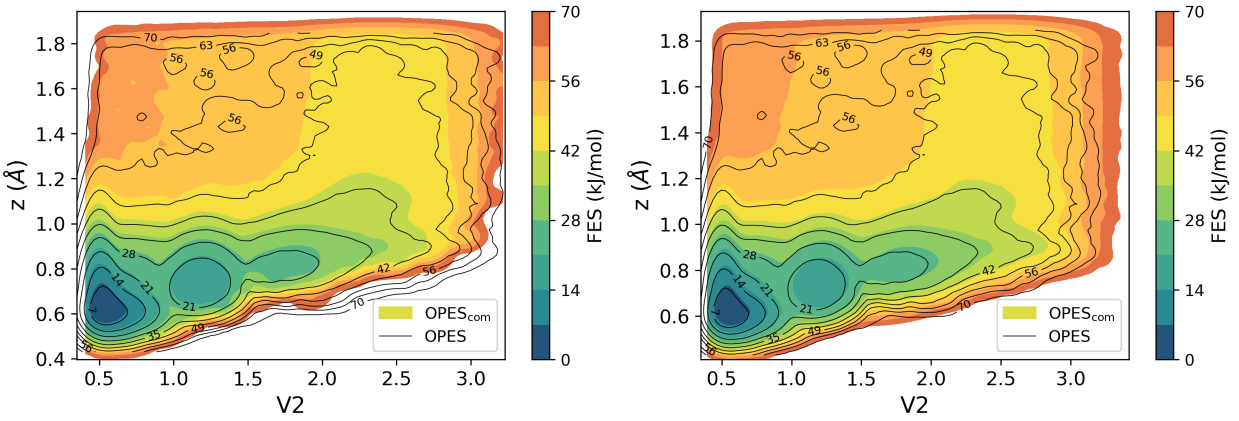

Figure S22: Results of the free energy landscape for the G3 guest binding to the OAH host. The captions of the subfigures are identical to Fig. S6

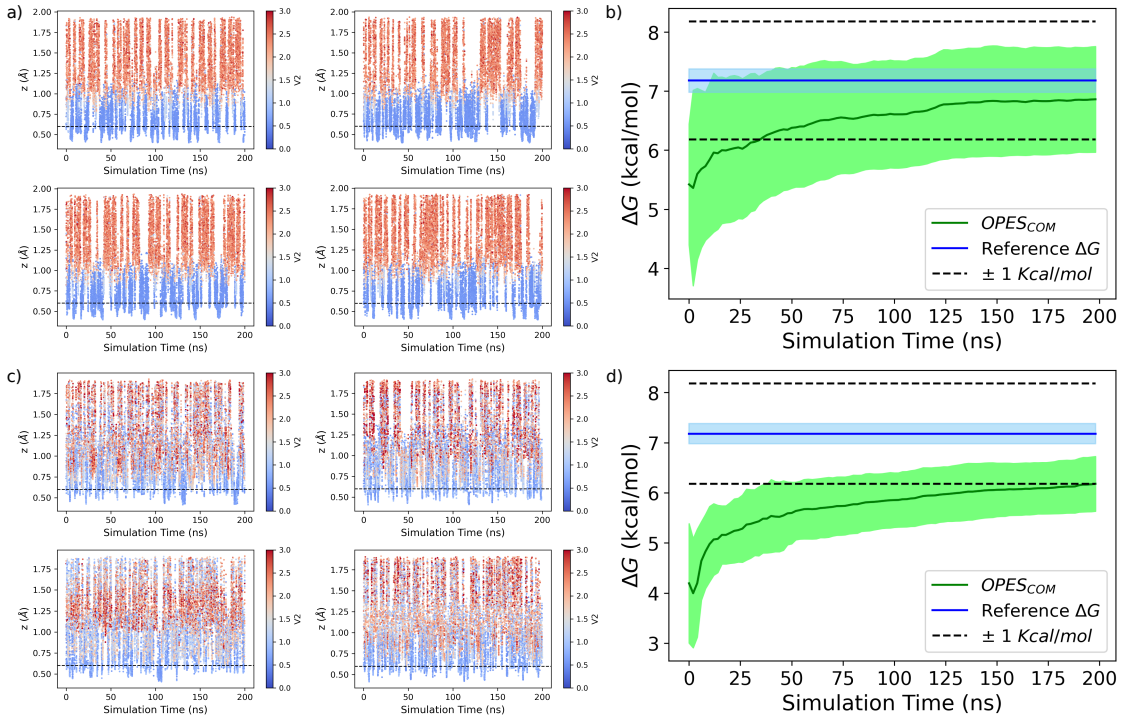

Figure S23: Back–and–forth transitions between the bound and unbound states for all the $OPES_{COM}$ simulations, along with the corresponding convergence profiles of the binding free energies. The subfigure captions are identical to Fig.S7

2.13 OAH-G4

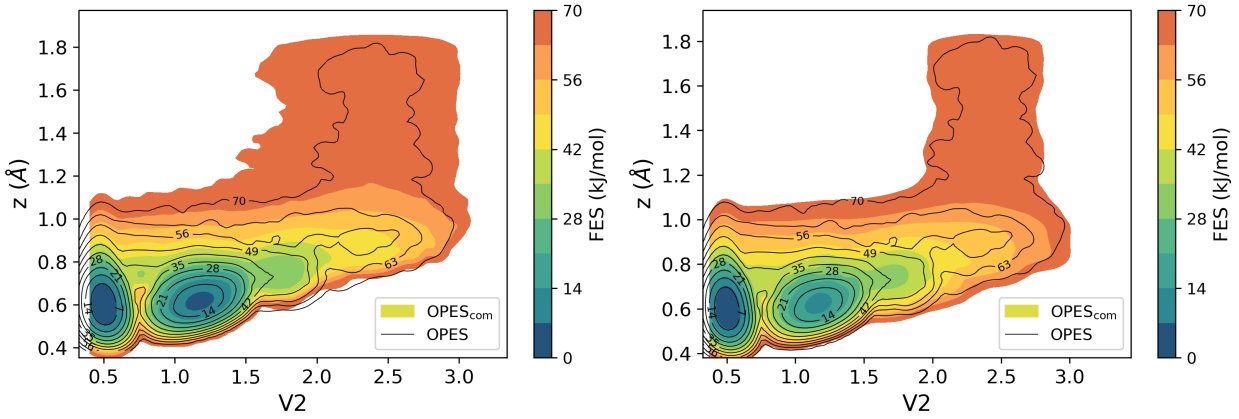

Figure S24: Results of the free energy landscape for the G4 guest binding to the OAH host. The captions of the subfigures are identical to Fig. S6

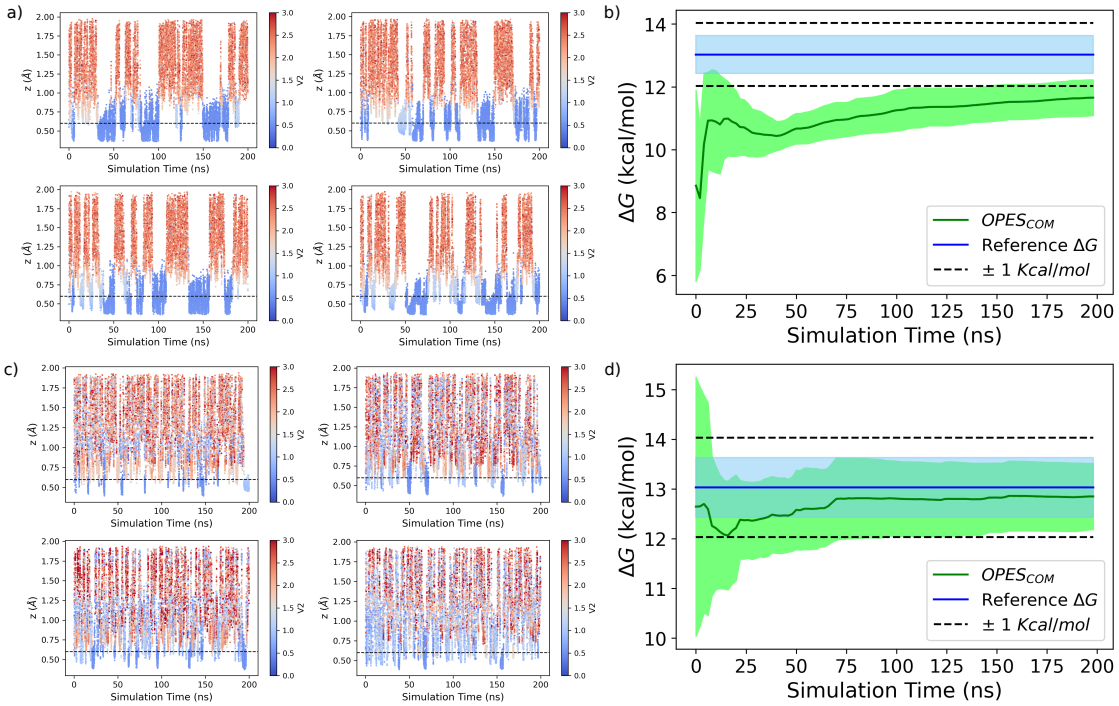

Figure S25: Back–and–forth transitions between the bound and unbound states for all the OPES$_{COM}$ simulations, along with the corresponding convergence profiles of the binding free energies. The subfigure captions are identical to Fig.S7

2.14 OAH-G5

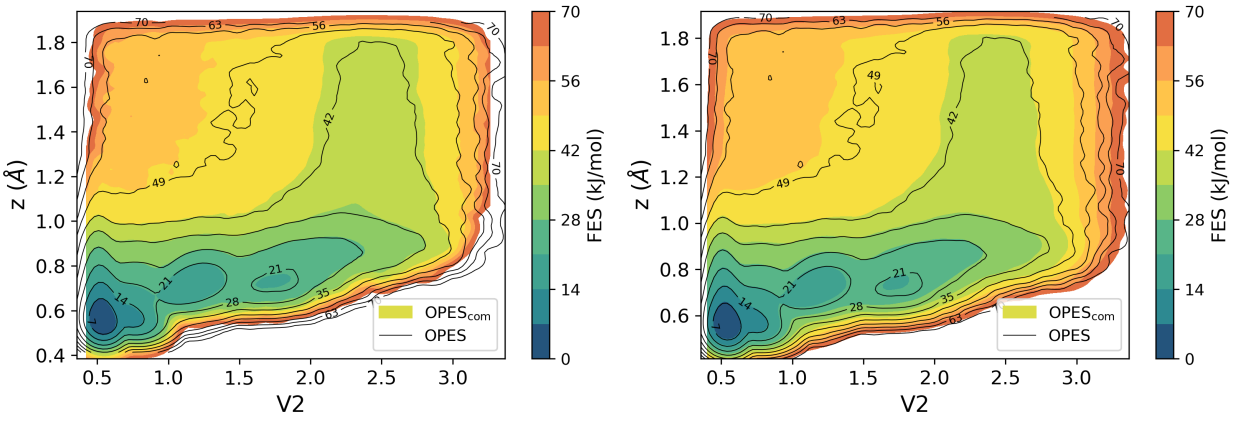

Figure S26: Results of the free energy landscape for the G5 guest binding to the OAH host. The captions of the subfigures are identical to Fig. S6

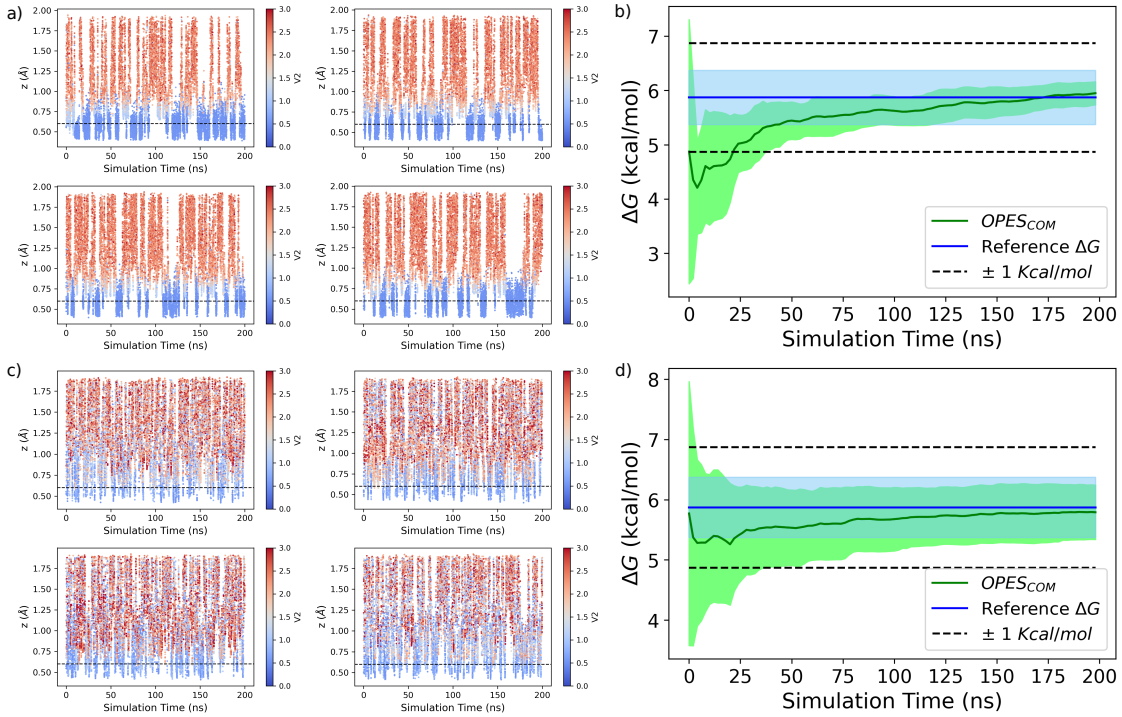

Figure S27: Back–and–forth transitions between the bound and unbound states for all the $OPES_{COM}$ simulations, along with the corresponding convergence profiles of the binding free energies. The subfigure captions are identical to Fig.S7

2.15 OAH-G6

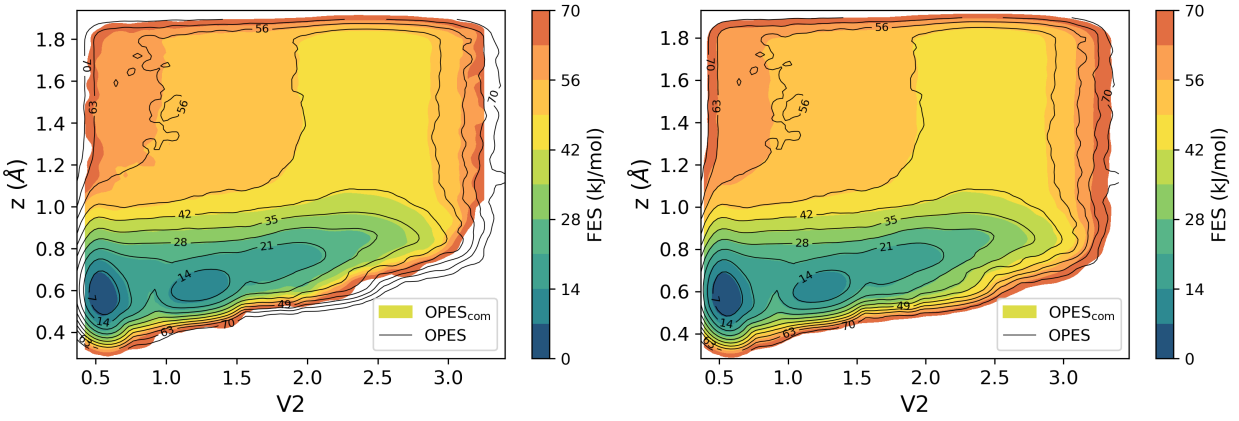

Figure S28: Results of the free energy landscape for the G6 guest binding to the OAH host. The captions of the subfigures are identical to Fig. S6

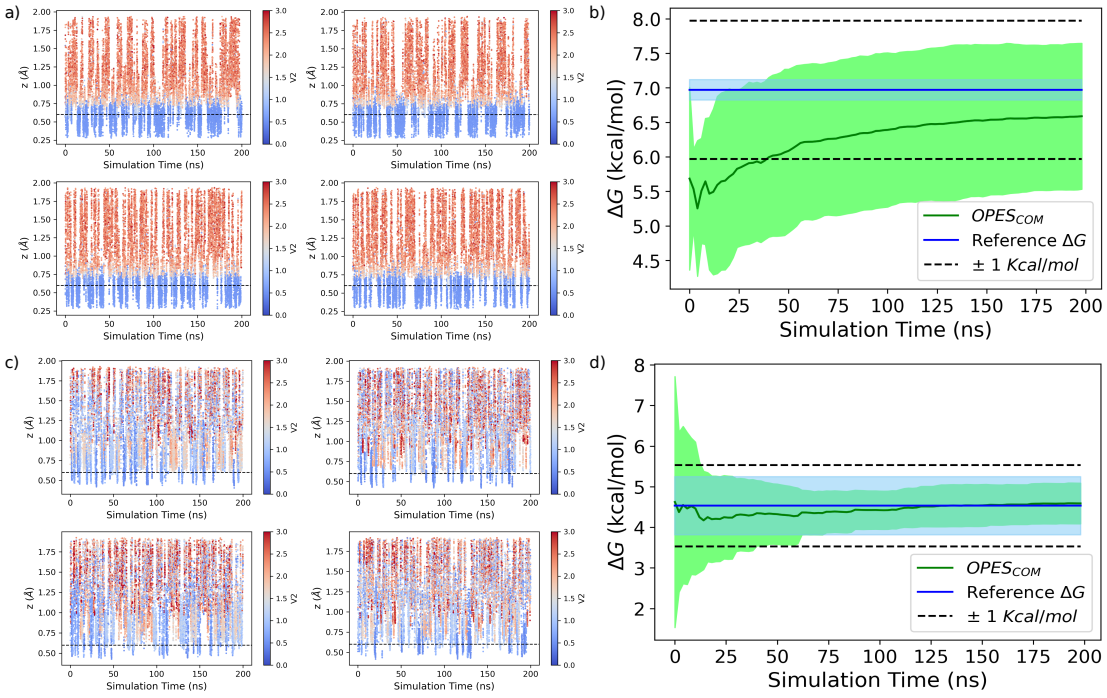

Figure S29: Back–and–forth transitions between the bound and unbound states for all the OPES$_{\text{COM}}$ simulations, along with the corresponding convergence profiles of the binding free energies. The subfigure captions are identical to Fig.S7